Bias Estimation and Observability for Optical Sensor Measurements with Targets of Opportunity

DJEDJIGA BELFADEL
RICHARD W. OSBORNE, III
YAAKOV BAR-SHALOM

In order to carry out data fusion, registration error correction is crucial in multisensor systems. This requires estimation of the sensor measurement biases. It is important to correct for these bias errors so that the multiple sensor measurements and/or tracks can be referenced as accurately as possible to a common tracking coordinate system. This paper provides a solution for bias estimation of multiple passive sensors using common targets of opportunity. The measurements provided by these sensors are assumed time-coincident (synchronous) and perfectly associated. The Line of Sight (LOS) measurements from the sensors can be fused into "composite" measurements, which are Cartesian target positions, i.e., linear in the target state. We evaluate the Cramér-Rao Lower Bound (CRLB) on the covariance of the bias estimates, which serves as a quantification of the available information about the biases. Statistical tests on the results of simulations show that this method is statistically efficient, even for small sample sizes (as few as three sensors and three points on the trajectory of a single target of opportunity). We also show that the Root Mean Squared (RMS) position error is significantly improved with bias estimation compared with the target position estimation using the original biased measurements. Bias observability issues, which arise in the case of two sensors, are also discussed.

Manuscript received August 12, 2013; revised November 18, 2013 and February 13, 2014; released for publication April 14, 2014.

Refereeing of this contribution was handled by Ramona Georgescu.

Funding provided by ARO W911NF-10-1-0369.

Authors' address: Electrical and Computer Engineering, University of Connecticut, Storrs, CT, U.S.A. Email: (djedjiga.belfadel@uconn.edu, rosborne@engr.uconn.edu, ybs@engr.uconn.edu)

I. INTRODUCTION

Multisensor systems use fusion of data from multiple sensors to form accurate estimates of a target track. To fuse multiple sensor data the individual sensor data must be expressed in a common reference frame. A problem encountered in multisensor systems is the presence of errors due to sensor bias. Some sources of bias errors include: measurement biases due to the deterioration of initial sensor calibration over time; attitude errors caused by biases in the gyros of the inertial measurement units of (airborne, seaborne, or spaceborne) sensors; and timing errors due to the biases in the onboard clock of each sensor platform [11].

The effect of biases introduced in the process of converting sensor measurements from polar (or spherical) coordinates to Cartesian coordinates has been discussed extensively in [2] together with the limit of validity of the standard transformation. If the conversion process is unbiased, the performance of a converted measurement Kalman filter is superior to a mixed coordinate Extended Kalman Filter EKF (i.e., target motion in Cartesian coordinates and measurements in polar coordinates) [2]. The approaches for conversion include the conventional conversion, the Unbiased Converted Measurement (UCM), the Modified Unbiased Converted Measurement (MUCM), and the Unscented Transform (UT). Recently, a decorrelated version of the UCM technique (DUCM) has been developed to address both conversion and estimation bias [8], [9]. Another example of biased measurement conversion is the estimation of range-rate from a moving platform. To measure range rate using the Doppler effect, it is necessary to nullify the impact of platform motion. The conventional nullification approach suffers from a similar bias problem as the position measurement conversion [3]. A novel scheme was proposed in [6] and [7] by applying the DUCM technique to own-Doppler nullification to eliminate this bias.

Time varying bias estimation based on a nonlinear least squares formulation and the singular value decomposition using truth data was presented in [11]. However, this work did not discuss the CRLB for bias estimation. An approach using Maximum a Posteriori (MAP) data association for concurrent bias estimation and data association based on sensor-level track state estimates was proposed in [12] and extended in [13]. Estimation of location biases only for passive sensors was discussed in [10]. The estimation of range, azimuth, and location biases for active sensors was presented in [14].

For angle-only sensors, imperfect registration leads to LOS angle measurement biases in azimuth and elevation. If uncorrected, registration error can lead to large tracking errors and potentially to the formation of multiple tracks (ghosts) on the same target.

In the present paper, bias estimation is investigated when only targets of opportunity are available. We assume the sensors are synchronized, their locations are

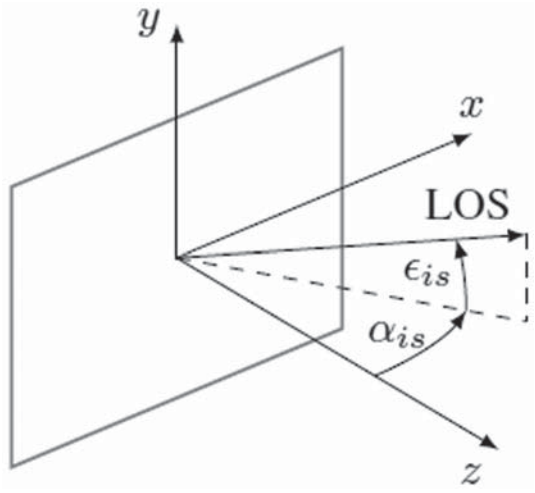

Fig. 1. Optical sensor coordinate system with the origin in the center of the focal plane.

fixed and known, the data association is correct, and we estimate their orientation biases. We investigate the use of the minimum possible number of optical sensors (which can not be less than two sensors). Two cases are considered. In the first case we use three optical sensors to observe three points on the trajectory of a single target of opportunity [4], in the second case we estimate the position of six points on the trajectory of a single target of opportunity simultaneously with the biases of two optical sensors [3]. First, we discuss the observability issues related to the bias estimation. Namely, it is shown that for two fixed sensors there is an inherent ambiguity due to a certain rotation that does not affect the measurements, i.e., one can not have complete observability of the sensor biases with targets of opportunity. For three fixed sensors, the biases are completely observable. We evaluate the Cramér-Rao Lower Bound (CRLB) on the covariance of the bias estimates (for the observable biases), which is the quantification of the available information on the sensor biases and show via statistical tests that the estimation is statistically efficient—it meets the CRLB. Section II presents the problem formulation and solution in detail. Section III describes the simulations performed and gives the results. Finally, Section IV gives the conclusions.

II. PROBLEM FORMULATION

The fundamental frame of reference used in this paper is a 3D Cartesian Common Coordinate System (CCS) defined by the orthogonal set of unit vectors $\{e_x, e_y, e_z\}$. In a multisensor scenario, sensor platform s will typically have a sensor reference frame associated with it (measurement frame of the sensor) defined by the orthogonal set of unit vectors $\{e_{\xi_s}, e_{\eta_s}, e_{\zeta_s}\}$. The origin of the measurement frame of the sensor is a translation of the CCS origin, and its axes are rotated with respect to the CCS axes. The rotation between these frames can be described by a set of Euler angles. We will refer to these angles $\phi_s + \phi_s^n$, $\rho_s + \rho_s^n$, and $\psi_s + \psi_s^n$ of sensor s, as roll, pitch, and yaw respectively [11], where ϕ_s^n is the nominal roll angle, ϕ_s is the roll bias, etc.

Each angle defines a rotation about a prescribed axis, in order to align the sensor frame axes with the CCS axes. The xyz rotation sequence is chosen, which is accomplished by first rotating about the x axis by ϕ_s^n, then rotating about the y axis by ρ_s^n, and finally rotating about the z axis by ψ_s^n. The rotations sequence can be expressed by the matrices

$$\begin{aligned} T_s(\psi_s^n, \rho_s^n, \phi_s^n) &= T_z(\psi_s^n) \cdot T_y(\rho_s^n) \cdot T_x(\phi_s^n) \\ &= \begin{bmatrix} \cos\psi_s^n & \sin\psi_s^n & 0 \\ -\sin\psi_s^n & \cos\psi_s^n & 0 \\ 0 & 0 & 1 \end{bmatrix} \\ &\cdot \begin{bmatrix} \cos\rho_s^n & 0 & -\sin\rho_s^n \\ 0 & 1 & 0 \\ \sin\rho_s^n & 0 & \cos\rho_s^n \end{bmatrix} \\ &\cdot \begin{bmatrix} 1 & 0 & 0 \\ 0 & \cos\phi_s^n & \sin\phi_s^n \\ 0 & -\sin\phi_s^n & \cos\phi_s^n \end{bmatrix} \end{aligned} \quad (1)$$

Assume there are N_S synchronized passive sensors with known fixed position in the CCS, $\boldsymbol{\xi}_s = [\xi_s, \eta_s, \zeta_s]'$, $s = 1, 2, \ldots, N_S$, and N_t targets, located at $\mathbf{x}_i = [x_i, y_i, z_i]'$, $i = 1, 2, \ldots, N_t$, in the same CCS. With the previous convention, the operations needed to transform the position of a given target i expressed in the CCS coordinate into the sensor s coordinate system is

$$\mathbf{x}_{is}^n = T(\boldsymbol{\omega}_s)(\mathbf{x}_i - \boldsymbol{\xi}_s), \quad i = 1, 2, \ldots, N_t, \quad s = 1, 2, \ldots, N_S \quad (2)$$

where $\boldsymbol{\omega}_s = [\phi_s^n, \rho_s^n, \psi_s^n]'$ is the nominal orientation of sensor s and $T(\boldsymbol{\omega}_s)$ is the appropriate rotation matrix and the translation is the difference between the vector position of the target i and the vector position of the sensor s, both expressed in the CCS. The superscript n in (2) indicates that the rotation matrix is based on the nominal sensor orientation.

As shown in Figure 1, the azimuth angle α_{is} is the angle in the sensor xz plane between the sensor z axis and the line of sight to the target, while the elevation angle ϵ_{is} is the angle between the line of sight to the target and its projection onto the xz plane, that is

$$\begin{bmatrix} \alpha_{is} \\ \epsilon_{is} \end{bmatrix} = \begin{bmatrix} \tan^{-1}\left(\dfrac{x_{is}}{z_{is}}\right) \\ \tan^{-1}\left(\dfrac{y_{is}}{\sqrt{x_{is}^2 + z_{is}^2}}\right) \end{bmatrix} \quad (3)$$

The model for the biased noise-free LOS measurements is then

$$\begin{bmatrix} \boldsymbol{\alpha}_{is}^b \\ \boldsymbol{\epsilon}_{is}^b \end{bmatrix} = \begin{bmatrix} g_1(\mathbf{x}_i, \boldsymbol{\xi}_s, \boldsymbol{\omega}_s, \mathbf{b}_s) \\ g_2(\mathbf{x}_i, \boldsymbol{\xi}_s, \boldsymbol{\omega}_s, \mathbf{b}_s) \end{bmatrix} = \mathbf{g}(\mathbf{x}_i, \boldsymbol{\xi}_s, \boldsymbol{\omega}_s, \mathbf{b}_s) \quad (4)$$

where g_1 and g_2 denote the sensor Cartesian coordinates-to-azimuth/elevation angle mapping that can be found by inserting equations (2) and (3) into (4). The bias vector of sensor s is

$$\mathbf{b}_s = [\phi_s, \rho_s, \psi_s]' \tag{5}$$

For a given target, each sensor provides the noisy LOS measurements

$$\mathbf{z}_{is} = \mathbf{g}(\mathbf{x}_i, \boldsymbol{\xi}_s, \boldsymbol{\omega}_s, \mathbf{b}_s) + \mathbf{w}_{is} \tag{6}$$

where

$$\mathbf{w}_{is} = [w_{is}^{\alpha}, w_{is}^{\epsilon}]' \tag{7}$$

The measurement noises $\mathbf{w}_{is}$ are zero-mean, white Gaussian with

$$R_s = \begin{bmatrix} (\sigma_s^{\alpha})^2 & 0 \\ 0 & (\sigma_s^{\epsilon})^2 \end{bmatrix} \tag{8}$$

and are assumed mutually independent.

The problem is to estimate the bias vectors for all sensors and the positions of the targets of opportunity. We shall obtain the Maximum Likelihood (ML) estimate of the augmented parameter vector

$$\boldsymbol{\theta} = [\mathbf{x}_1', \ldots, \mathbf{x}_{N_t}', \mathbf{b}_1', \ldots, \mathbf{b}_{N_S}']' \tag{9}$$

consisting of the (unknown) position of target i and the biases of sensor s, $i = 1, \ldots, N_t, s = 1, \ldots, N_S$, by maximizing the likelihood function

$$\Lambda(\boldsymbol{\theta}) = \prod_{i=1}^{N_t} \prod_{s=1}^{N_S} p(\mathbf{z}_{is} \mid \boldsymbol{\theta}) \tag{10}$$

where

$$p(\mathbf{z}_{is} \mid \boldsymbol{\theta}) = |2\pi R_s|^{-1/2} \cdot \exp(-\tfrac{1}{2}[\mathbf{z}_{is} - \mathbf{h}_{is}(\boldsymbol{\theta})]' R_s^{-1} [\mathbf{z}_{is} - \mathbf{h}_{is}(\boldsymbol{\theta})]) \tag{11}$$

and

$$\mathbf{h}_{is}(\boldsymbol{\theta}) \triangleq \mathbf{g}(\mathbf{x}_i, \boldsymbol{\xi}_s, \boldsymbol{\omega}_s, \mathbf{b}_s) \tag{12}$$

The ML Estimate (MLE) is then

$$\hat{\boldsymbol{\theta}}^{ML} = \arg\max_{\boldsymbol{\theta}} \Lambda(\boldsymbol{\theta}) \tag{13}$$

In order to find the MLE, one has to solve a nonlinear least squares problem for the exponent in (11). This will be done using a numerical search via the Iterated Least Squares (ILS) technique [1].

A. Requirements for Bias Estimability

First requirement for bias estimability. For a given target we have a two-dimensional measurement from each sensor (the two LOS angles to the target). We assume that each sensor sees all the targets at a common time.[1] Stacking together each measurement of N_t targets seen by N_S sensors results in an overall measurement vector of dimension $2N_tN_S$. Given that the position and bias vectors of each target are three-dimensional, and knowing that the number of equations (size of the stacked measurement vector) has to be at least equal to the number of parameters to be estimated (target positions and biases), we must have

$$2N_tN_S \geq 3(N_t + N_S) \tag{14}$$

This is a necessary condition but not sufficient because (13) has to have a unique solution, i.e., the parameter vector has to be estimable. This is guaranteed by the second requirement.

Second requirement of bias estimability. This is the invertibility of the Fisher Information Matrix (FIM) [1], to be discussed later. For example, to estimate the biases of 3 sensors (9 bias components) we need 3 targets (9 position components), i.e., the search is in an 18-dimensional space. In order to estimate the biases of 2 sensors (6 bias components) we need at least 6 targets (18 position components) to meet the necessary requirement (14). The rank of the FIM has to be equal to the number of parameters to be estimated (6 + 18 = 24). The full rank of the FIM is a necessary and sufficient condition for estimability, however, for the two fixed sensors situation this is not satisfied. This issue will be discussed further in the section III.B, where an explanation will be provided.

B. Iterated Least Squares

Given the estimate $\hat{\boldsymbol{\theta}}^j$ after j iterations, the ILS estimate after the $(j+1)$th iteration will be

$$\hat{\boldsymbol{\theta}}^{j+1} = \hat{\boldsymbol{\theta}}^j + [(H^j)' R^{-1} H^j]^{-1} (H^j)' R^{-1} [\mathbf{z} - \mathbf{h}(\hat{\boldsymbol{\theta}}^j)] \tag{15}$$

where

$$\mathbf{z} = [z_{11}', \ldots, z_{is}', \ldots, z_{N_tN_S}']' \tag{16}$$

$$\mathbf{h}(\hat{\boldsymbol{\theta}}^j) = [h_{11}(\hat{\boldsymbol{\theta}}^j)', \ldots, h_{is}(\hat{\boldsymbol{\theta}}^j)', \ldots, h_{N_tN_S}(\hat{\boldsymbol{\theta}}^j)'] \tag{17}$$

R is a block diagonal matrix consisting of N_t blocks of N_S blocks of R_s

$$H^j = \left. \frac{\partial \mathbf{h}(\boldsymbol{\theta}^j)}{\partial \boldsymbol{\theta}} \right|_{\boldsymbol{\theta} = \hat{\boldsymbol{\theta}}^j} \tag{18}$$

is the Jacobian matrix of the vector consisting of the stacked measurement functions (17) w.r.t. (9) evaluated at the ILS estimate from the previous iteration j. In this case, the Jacobian matrix is, with the iteration index omitted for conciseness,

$$H = [H_{11} \quad H_{21} \cdots H_{N_t1} \quad H_{12} \cdots H_{N_tN_S}]' \tag{19}$$

[1]This can also be the same target at different times, as long as the sensors are synchronized.

where

$$H'_{is} = \begin{bmatrix} \frac{\partial g_{1_{is}}}{\partial x_1} & \frac{\partial g_{2_{is}}}{\partial x_1} \\ \frac{\partial g_{1_{is}}}{\partial y_1} & \frac{\partial g_{2_{is}}}{\partial y_1} \\ \frac{\partial g_{1_{is}}}{\partial z_1} & \frac{\partial g_{2_{is}}}{\partial z_1} \\ \vdots & \vdots \\ \frac{\partial g_{1_{is}}}{\partial x_{N_t}} & \frac{\partial g_{2_{is}}}{\partial x_{N_t}} \\ \frac{\partial g_{1_{is}}}{\partial y_{N_t}} & \frac{\partial g_{2_{is}}}{\partial y_{N_t}} \\ \frac{\partial g_{1_{is}}}{\partial z_{N_t}} & \frac{\partial g_{2_{is}}}{\partial z_{N_t}} \\ \frac{\partial g_{1_{is}}}{\partial \psi_1} & \frac{\partial g_{2_{is}}}{\partial \psi_1} \\ \frac{\partial g_{1_{is}}}{\partial \rho_1} & \frac{\partial g_{2_{is}}}{\partial \rho_1} \\ \frac{\partial g_{1_{is}}}{\partial \phi_1} & \frac{\partial g_{2_{is}}}{\partial \phi_1} \\ \vdots & \vdots \\ \frac{\partial g_{1_{is}}}{\partial \psi_{N_S}} & \frac{\partial g_{2_{is}}}{\partial \psi_{N_S}} \\ \frac{\partial g_{1_{is}}}{\partial \rho_{N_S}} & \frac{\partial g_{2_{is}}}{\partial \rho_{N_S}} \\ \frac{\partial g_{1_{is}}}{\partial \phi_{N_S}} & \frac{\partial g_{2_{is}}}{\partial \phi_{N_S}} \end{bmatrix} \tag{20}$$

The appropriate partial derivatives are given in the Appendix.

C. Initialialization

In order to perform the numerical search via ILS, an initial estimate $\hat{\boldsymbol{\theta}}^0$ is required. Assuming that the biases are null, the LOS measurements from the first and the second sensor α_{i1}, α_{i2} and ϵ_{i1} can be used to solve for each initial Cartesian target position, in the CCS, as

$$x_i^0 = \frac{\xi_2 - \xi_1 + \zeta_1 \tan\alpha_{i1} - \zeta_2 \tan\alpha_{i2}}{\tan\alpha_{i1} - \tan\alpha_{i2}} \tag{21}$$

$$y_i^0 = \frac{\tan\alpha_{i1}(\xi_2 + \tan\alpha_{i2}(\zeta_1 - \zeta_2)) - \xi_1 \tan\alpha_{i2}}{\tan\alpha_{i1} - \tan\alpha_{i2}} \tag{22}$$

$$z_i^0 = \eta_1 + \tan\epsilon_{i1} \left| \frac{(\xi_1 - \xi_2)\cos\alpha_{i2} + (\zeta_2 - \zeta_1)\sin\alpha_{i2}}{\sin(\alpha_{i1} - \alpha_{i2})} \right| \tag{23}$$

D. Cramér-Rao Lower Bound

In order to evaluate the efficiency of the estimator, the CRLB must be calculated. The CRLB provides a lower bound on the covariance matrix of an unbiased estimator as [1]

$$E\{(\boldsymbol{\theta} - \hat{\boldsymbol{\theta}})(\boldsymbol{\theta} - \hat{\boldsymbol{\theta}})'\} \geq J^{-1} \tag{24}$$

where J is the Fisher Information Matrix (FIM), $\boldsymbol{\theta}$ is the true parameter vector to be estimated, and $\hat{\boldsymbol{\theta}}$ is the estimate. The FIM is

$$J = E\{[\nabla_{\boldsymbol{\theta}} \ln\Lambda(\boldsymbol{\theta})][\nabla_{\boldsymbol{\theta}} \ln\Lambda(\boldsymbol{\theta})]'\}|_{\boldsymbol{\theta}=\boldsymbol{\theta}_{\text{true}}} \tag{25}$$

where the gradient of the log-likelihood function is

$$\lambda(\boldsymbol{\theta}) \triangleq \ln\Lambda(\boldsymbol{\theta}) \tag{26}$$

$$\nabla_{\boldsymbol{\theta}}\lambda(\boldsymbol{\theta}) = \sum_{i=1}^{N_t}\sum_{s=1}^{N_S} H'_{is} R_{is}^{-1}(\mathbf{z}_{is} - \mathbf{h}_{is}(\boldsymbol{\theta})) \tag{27}$$

which, when plugged into (25), gives

$$\begin{aligned} J &= \sum_{i=1}^{N_t}\sum_{s=1}^{N_S} H'_{is}(R_s^{-1})H_{is}|_{\theta=\boldsymbol{\theta}_{\text{true}}} \\ &= H'(R^{-1})H|_{\boldsymbol{\theta}=\boldsymbol{\theta}_{\text{true}}} \end{aligned} \tag{28}$$

III. SIMULATIONS

A. Three-Sensor Case

We simulated three optical sensors at various fixed and known locations observing a target at three points in time at unknown locations (which is equivalent to viewing three different targets at unknown locations). Five scenarios of three sensors are examined for a set of target locations. They are shown in Figures 2–6. Each scenario is such that each target position can be observed by all sensors. As discussed in the previous section, the three sensor biases were roll, pitch, and yaw angle offsets. The biases for each sensor were set to $1^\circ = 17.45$ mrad. We made 100 Monte Carlo runs for each scenario. In order to establish a baseline for evaluating the performance of our algorithm, we also ran the simulations without biases and with biases, but without bias estimation. The horizontal and vertical Fields of View (FOV) of each sensor are assumed to be 60°. The measurement noise standard deviation σ_s (identical across sensors for both azimuth and elevation measurements) was assumed to be 0.34 mrad (based on an assumed pixel subtended angle of 0.02° (a modest 9 megapixel FPA with FOV $60^\circ \cdot 60^\circ$; $60^\circ/\sqrt{9 \cdot 10^6} = 0.02^\circ$).

1) Description of the Scenarios. The sensors are assumed to provide LOS angle measurements. We denote by $\boldsymbol{\xi}_1, \boldsymbol{\xi}_2, \boldsymbol{\xi}_3$ the 3D Cartesian sensor positions, and $\mathbf{x}_1, \mathbf{x}_2, \mathbf{x}_3$ the 3D Cartesian target positions (all in CCS). The three target positions are the same for all the scenarios, and they were chosen from a trajectory of a ballistic

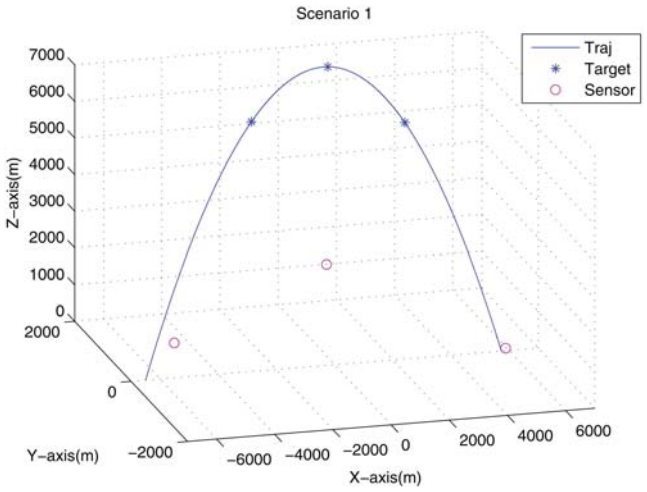

Fig. 2. Scenario 1.

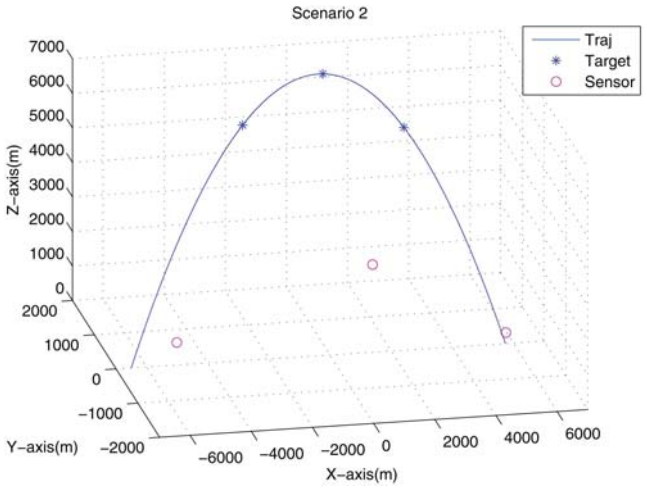

Fig. 3. Scenario 2.

target as follows (in m)

$$\mathbf{x}_1 = [-2860, 0, 6820]' \tag{29}$$

$$\mathbf{x}_2 = [-235.9, 0, 8152]' \tag{30}$$

$$\mathbf{x}_3 = [2413, 0, 6451]' \tag{31}$$

Table I summarizes the sensor positions (in m) for the five scenarios considered.

2) Statistical Efficiency of the Estimates. In order to test for the statistical efficiency of the estimate (of the 18 dimensional vector (9)), the Normalized Estimation Error Squared (NEES) [1] is used, with the CRLB as the covariance matrix. The sample average NEES over 100 Monte Carlo runs is shown in Figure 7 for all scenarios. The NEES is calculated using the FIM evaluated at both the true bias values and target positions, as well as at the estimated biases and target positions. According to the CRLB, the FIM has to be evaluated at the true parameter. Since this is not available in practice, however, it is useful to evaluate the FIM also at the estimated parameter, the only one available in real world

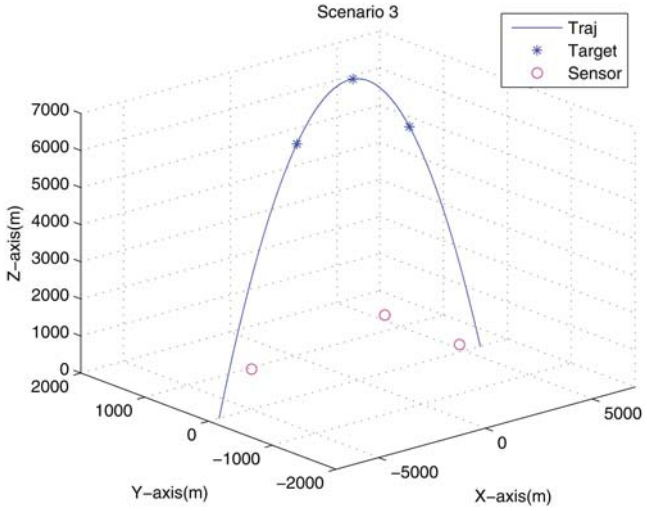

Fig. 4. Scenario 3.

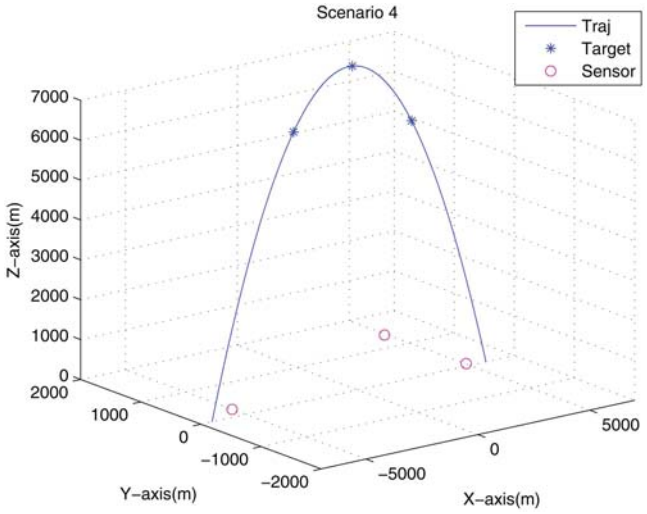

Fig. 5. Scenario 4.

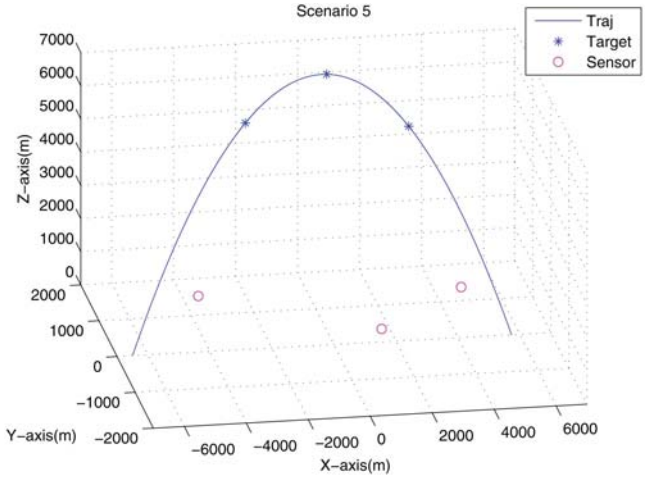

Fig. 6. Scenario 5.

implementations [15], [16]. The results are practically identical regardless of which values are chosen for evaluation of the FIM. The 95% probability region for the

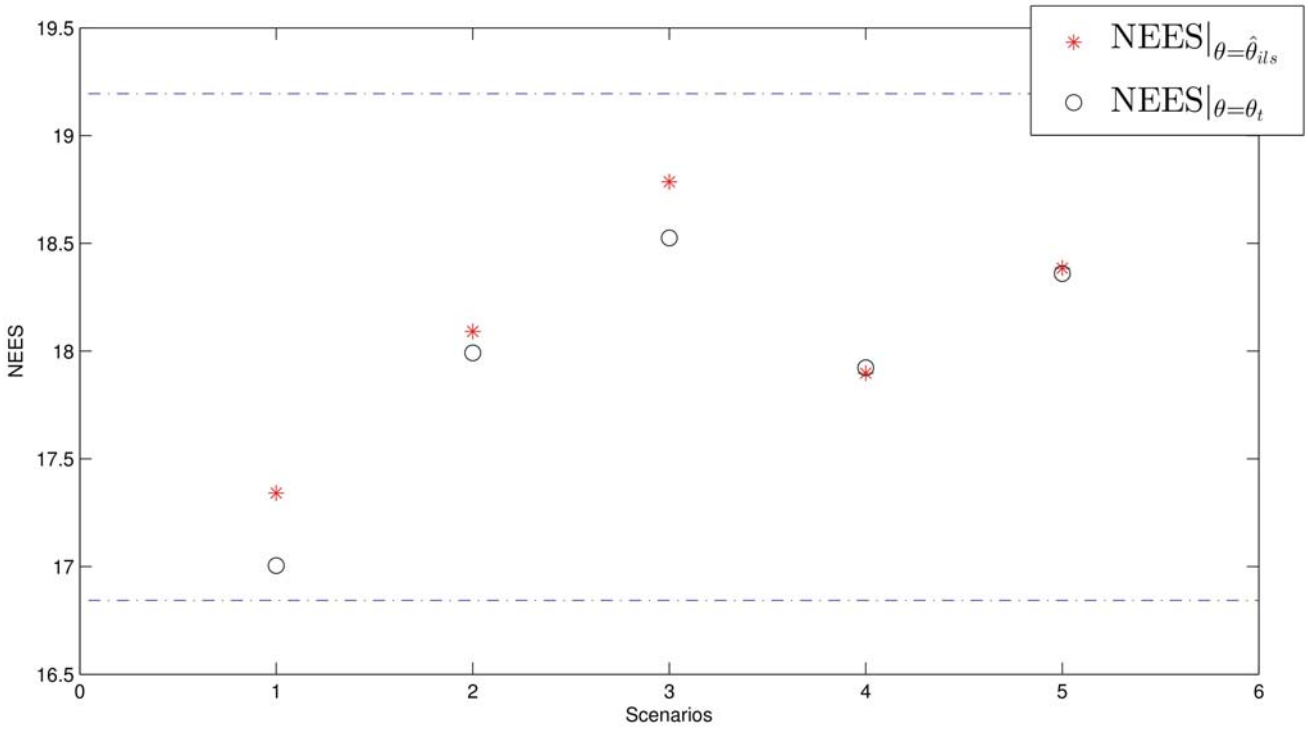

Fig. 7. Sample average NEES over 100 Monte Carlo runs for all five scenarios (three-sensor case).

TABLE I
Sensor positions (in m) for the scenarios considered.

Scenario	First Sensor			Second Sensor			Third Sensor		
	ξ	η	ζ	ξ	η	ζ	ξ	η	ζ
1	−5500	15	950	−230	45	2720	5900	20	50
2	−4900	145	505	1230	−220	2765	5900	200	110
3	−4900	25	1050	1330	25	1585	4900	45	150
4	−5600	5	200	1230	10	1220	4900	20	50
5	−3500	1500	25	1230	−520	1265	4900	1350	20

TABLE II
Sample average position RMSE (in m) for the three targets, over 100 Monte Carlo runs, for the three estimation schemes (three-sensor case).

Scheme	First Target	Second Target	Third Target
	RMSE	RMSE	RMSE
1	3.33	3.51	2.82
2	146.61	167.43	134.80
3	38.93	43.82	37.68

100 sample average NEES of the 18 dimensional parameter vector is [16.84, 19.19]. For all five scenarios, the NEES is found to be within this interval and the MLE is therefore statistically efficient. Figure 8 shows the individual bias component NEES for all scenarios, The 95% probability region for the 100 sample average single component NEES is [0.74, 1.29]. For all five scenarios these NEES are found to be within this interval.

The RMS position errors for the three targets are summarized in Table II. In this table, the first estimation scheme was established as a baseline using bias-free LOS measurements to estimate the target positions.[2] For the second scheme, we used biased LOS measurements but we only estimated target positions. In the last scheme, we used biased LOS measurements and we simultaneously estimated the target positions and sensor biases. Bias estimation yields significantly improved target RMS position errors in the presence of biases.

Each component of $\boldsymbol{\theta}$ should also be individually consistent with its corresponding σ_{CRLB} (the square root of the corresponding diagonal element of the inverse of FIM). In this case, the sample average bias RMSE over 100 Monte Carlo runs should be within 15% of its corresponding bias standard deviation from the

[2] As shown in [15], [16] the unbiased LOS measurements yield composite measurements (full position MLEs) whose errors are zero-mean and their covariance is equal to the corresponding CRLB.

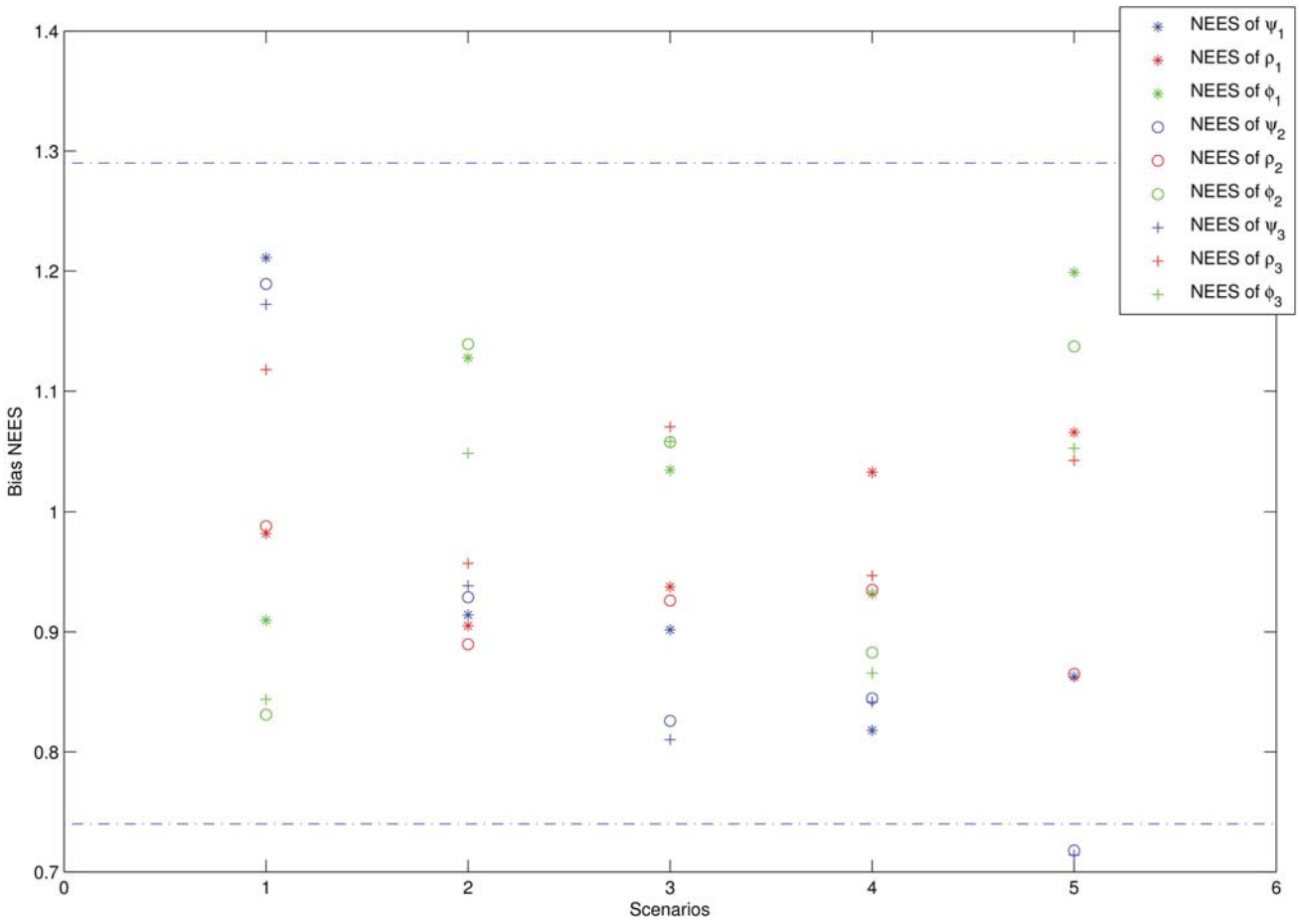

Fig. 8. Sample average bias NEES (CRLB evaluated at the estimate), for each of the 9 biases, over 100 Monte Carlo runs for all five scenarios (three-sensor case).

TABLE III
Sample average bias RMSE over 100 Monte Carlo runs and the corresponding bias standard deviation from the CRLB (σ_{CRLB}), for all configurations (in mrad) (three-sensor case).

Scenario		First Sensor			Second Sensor			Third Sensor		
		ψ	ρ	ϕ	ψ	ρ	ϕ	ψ	ρ	ϕ
1	RMSE	3.168	1.173	2.558	7.358	1.121	3.321	3.210	1.419	2.261
	σ_{CRLB}	2.872	1.183	2.679	6.721	1.129	3.639	2.954	1.341	2.459
2	RMSE	1.935	1.133	2.642	7.573	1.069	3.352	4.224	1.335	1.881
	σ_{CRLB}	2.028	1.190	2.485	7.855	1.129	3.138	4.355	1.362	1.835
3	RMSE	2.473	1.089	5.923	6.475	1.084	6.675	4.504	1.266	5.272
	σ_{CRLB}	2.600	1.124	5.780	7.054	1.140	6.455	4.969	1.239	5.105
4	RMSE	2.512	1.257	5.950	6.472	1.161	6.522	4.579	1.351	5.218
	σ_{CRLB}	2.801	1.243	6.198	7.094	1.201	6.976	5.024	1.388	5.634
5	RMSE	3.102	1.697	4.418	5.979	2.124	5.609	4.238	2.195	3.979
	σ_{CRLB}	3.334	1.646	4.034	7.078	2.295	5.253	5.011	2.150	3.869

CRLB with 95% probability. Table III demonstrates the consistency of the individual bias estimates. This complements the NEES evaluations from Figure 8.

To confirm that the bias estimates are unbiased, the average bias error $\bar{\tilde{b}}$, from Table IV, over 100 Monte Carlo runs confirms that $|\bar{\tilde{b}}|$ is less then $2\sigma_{\text{CRLB}}/\sqrt{N}$ (which it should be with 95% probability), i.e., these bias estimates are unbiased.

In order to examine the statistical efficiency for a variety of target-sensor geometries, the sensors' locations were varied from one scenario to another in order to vary the Geometric Dilution of Precision (GDOP),

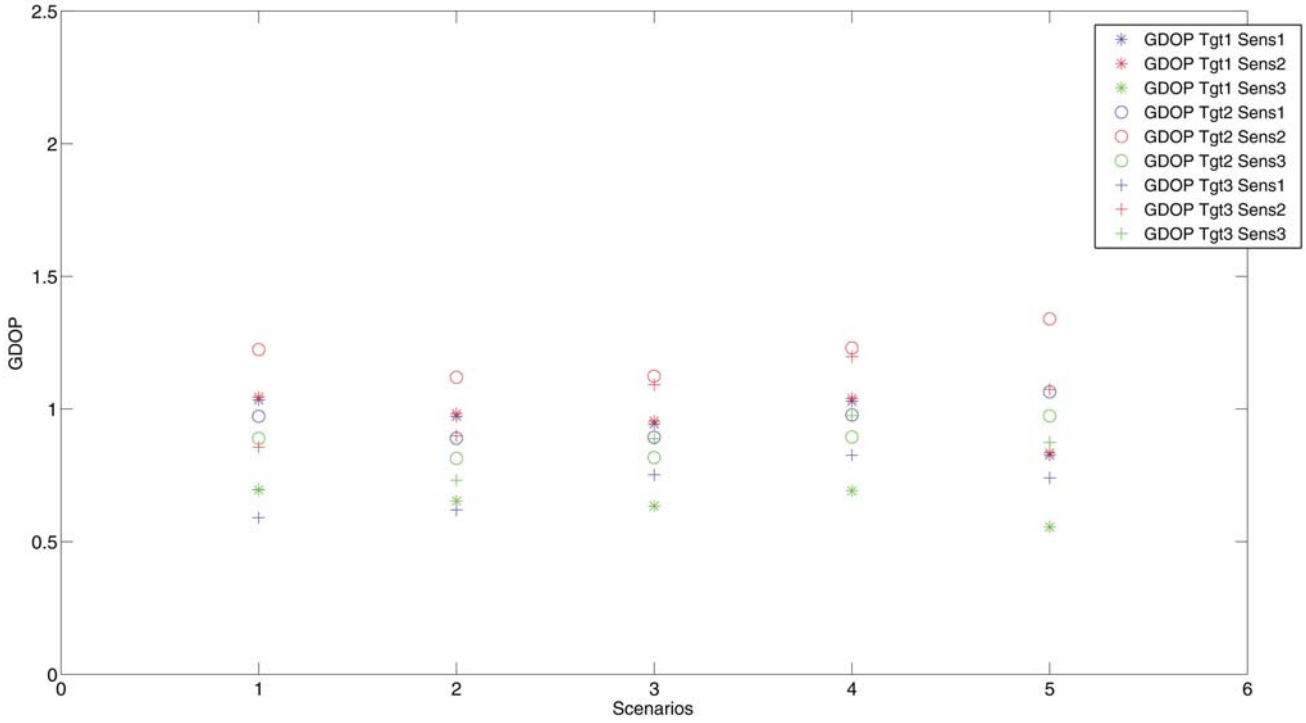

Fig. 9. GDOPs for the five scenarios considered (three-sensor case).

TABLE IV

Sample average bias error $\bar{\tilde{b}}$ over $N = 100$ Monte Carlo runs for all configurations (in mrad) (to confirm that the bias estimates are unbiased) (three-sensor case).

Scenario		First Sensor			Second Sensor			Third Sensor		
		ψ	ρ	ϕ	ψ	ρ	ϕ	ψ	ρ	ϕ
1	$\bar{\tilde{b}}$	0.336	−0.076	0.034	0.693	−0.127	0.128	0.240	−0.111	0.146
	$\frac{\sigma_{\text{CRLB}}}{\sqrt{N}}$	0.287	0.118	0.268	0.672	0.113	0.364	0.295	0.134	0.246
2	$\bar{\tilde{b}}$	−0.099	0.012	0.045	−0.356	0.002	0.017	−0.195	0.088	−0.038
	$\frac{\sigma_{\text{CRLB}}}{\sqrt{N}}$	0.203	0.119	0.248	0.785	0.113	0.314	0.436	0.136	0.184
3	$\bar{\tilde{b}}$	−0.191	0.125	0.039	−0.565	0.134	−0.076	−0.348	0.198	−0.162
	$\frac{\sigma_{\text{CRLB}}}{\sqrt{N}}$	0.260	0.112	0.578	0.705	0.114	0.645	0.497	0.124	0.510
4	$\bar{\tilde{b}}$	0.020	−0.153	−0.481	0.412	−0.094	−0.374	0.345	−0.180	−0.209
	$\frac{\sigma_{\text{CRLB}}}{\sqrt{N}}$	0.280	0.124	0.620	0.709	0.120	0.698	0.502	0.139	0.563
5	$\bar{\tilde{b}}$	0.522	−0.002	−0.058	0.823	0.038	0.034	0.576	−0.009	0.025
	$\frac{\sigma_{\text{CRLB}}}{\sqrt{N}}$	0.333	0.165	0.403	0.708	0.230	0.525	0.501	0.215	0.387

defined as

$$\text{GDOP} \triangleq \frac{\text{RMSE}}{r\sqrt{\sigma_\alpha^2 + \sigma_\epsilon^2}} \tag{32}$$

where "RMSE" is the RMS position error for a target location (in the absence of biases), r is the range to the target, and σ_α and σ_ϵ are the azimuth and elevation measurement error standard deviations, respectively. Figure 9 shows the various GDOP levels in the 9 target-sensor combinations for each of the five scenarios for which statistical efficiency was confirmed.

B. Two-Sensor Case

We simulated two optical sensors at various fixed locations observing a target at six (unknown) locations (which is equivalent to viewing six different targets at unknown locations). In this case a 24-dimensional parameter vector is to be estimated.

It was observed that the rank of the FIM was 23 which implies incomplete observability. Even with more target points there was always a deficiency of 1 in the rank of the FIM. As shown in Figure 10, this can be

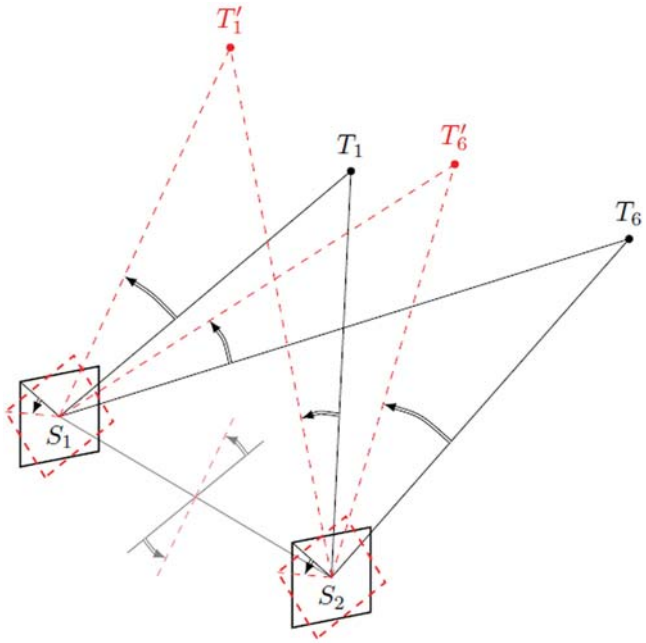

Fig. 10. Rotation around axis S_1S_2 of the sensors and all targets by the same angle leaves all the LOS angles from the sensors to the targets unchanged.

explained as follows: a rotation of the sensors and all the targets around the axis defined by the line S_1S_2 connecting the optical centers of the two sensors is not observable because this will yield the same measurements regardless of the magnitude of this rotation. Note that this rotation does not change the locations of the sensors, which are assumed known. Thus, with two sensors, one cannot estimate all 6 biases—we are limited to estimating 5 and this will be borne out by the FIM in the simulations. A similar observation was made in [5] for sensors that are facing each other. However the above discussion points out that the sensors do not have to face each other—there is an inherent lack of observability of any rotation around the above defined axis. This problem does not exist if there are three or more sensors[3] because there is no axis of rotation that does not change the location of at least one sensor.

Four scenarios of two sensors are examined for a set of target locations. They are shown in Figures 11–14. Each scenario is such that each target position can be observed by all sensors. As discussed in the previous section, the three sensor biases were roll, pitch, and yaw angle offsets. The second sensor roll bias is assumed to be known and null, this is in view of the above discussion about the inherent rank 1 deficiency of the FIM in the two sensors case which makes it impossible to estimate all the 6 sensor biases. Reducing the number of biases from 6 to 5 allows a full rank FIM. All the other biases for each sensor were set to $1^\circ = 17.45$ mrad.

We made 100 Monte Carlo runs for each scenario. In order to establish a baseline for evaluating the performance of our algorithm, we also ran the simulations without bias, and with bias but without bias estimation. The measurement noise standard deviation σ_s (identical across sensors for both azimuth and elevation measurements) was assumed to be 0.34 mrad. As a fifth scenario we simulated two optical sensors observing two targets (two trajectories) at three points in time for each target, as shown in Figure 15.

[3]Provided that the three sensors (or any number of) are not located in a straight line.

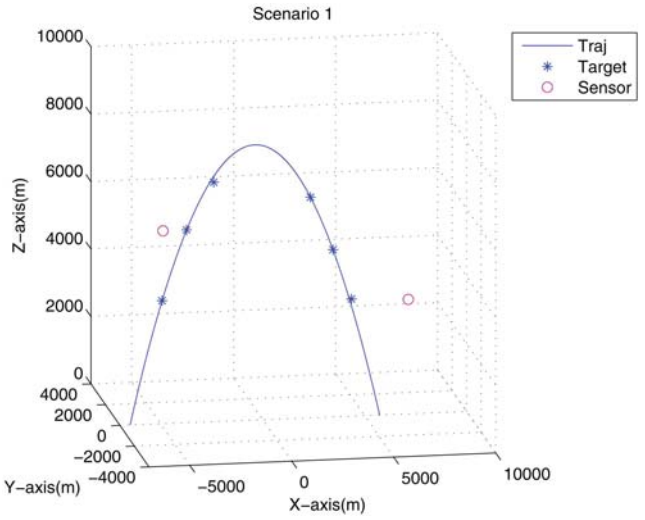

Fig. 11. Scenario 1 for the two-sensor case.

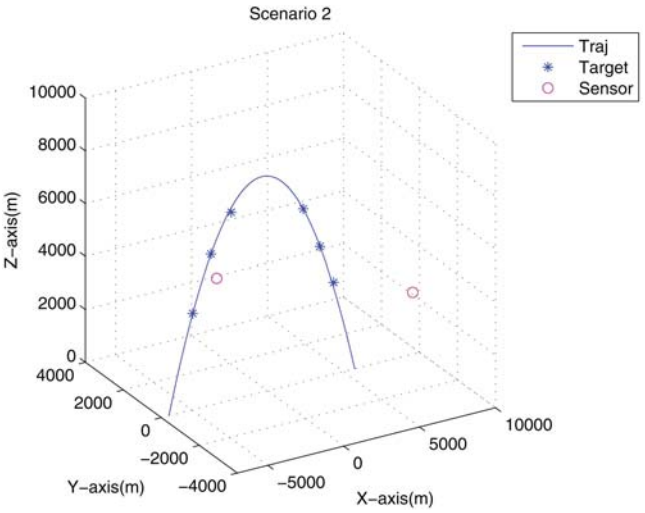

Fig. 12. Scenario 2 for the two-sensor case.

1) Description of the Scenarios. The sensors are assumed to provide LOS angle measurements. We denote by $\boldsymbol{\xi}_1, \boldsymbol{\xi}_2$ the 3D Cartesian sensor positions, and $\mathbf{x}_1, \mathbf{x}_2, \mathbf{x}_3, \mathbf{x}_4, \mathbf{x}_5, \mathbf{x}_6$ the 3D Cartesian target positions (all in CCS). The six target positions are the same for the first four scenarios, and they were chosen from a trajectory of a ballistic target as follows (in m)

$$\mathbf{x}_1 = [-4931, 0, 3649]' \tag{33}$$

$$\mathbf{x}_2 = [-3731, 0, 5714]' \tag{34}$$

$$\mathbf{x}_3 = [-2400, 0, 7100]' \tag{35}$$

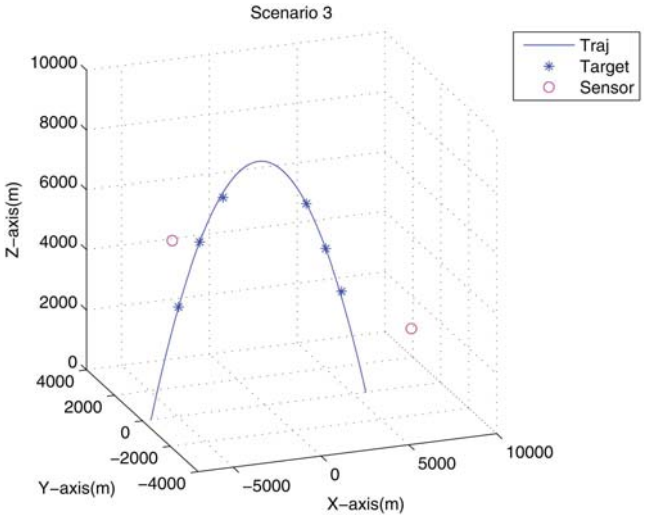

Fig. 13. Scenario 3 for the two-sensor case.

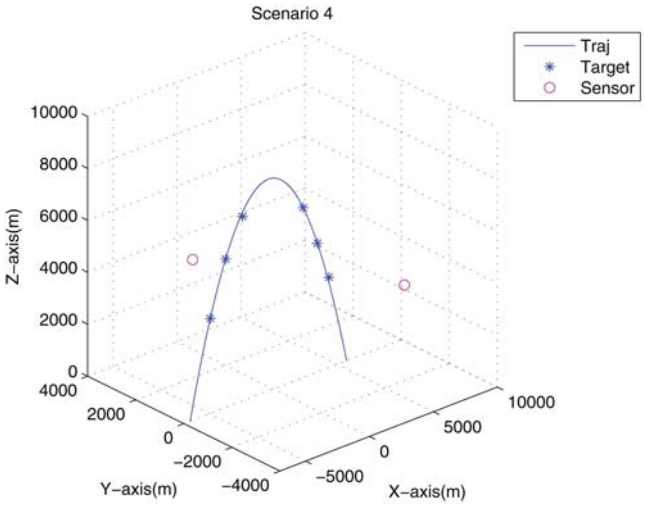

Fig. 14. Scenario 4 for the two-sensor case.

$$\mathbf{x}_4 = [2341, 0, 6538]' \tag{36}$$

$$\mathbf{x}_5 = [3448, 0, 4956]' \tag{37}$$

$$\mathbf{x}_6 = [4351, 0, 3475]' \tag{38}$$

For the fifth scenario, the six target positions were chosen from two trajectories of two ballistic targets as follows (in m)

$$\mathbf{x}_1 = [-4931, 0, 3649]' \tag{39}$$

$$\mathbf{x}_2 = [2994, 0, 5670]' \tag{40}$$

$$\mathbf{x}_3 = [-2400, 0, 7100]' \tag{41}$$

$$\mathbf{x}_4 = [-1400, 0, 7932]' \tag{42}$$

$$\mathbf{x}_5 = [2376, 0, 6497]' \tag{43}$$

$$\mathbf{x}_6 = [4075, 0, 3823]' \tag{44}$$

Table V summarizes the sensor positions (in m) for the five scenarios considered.

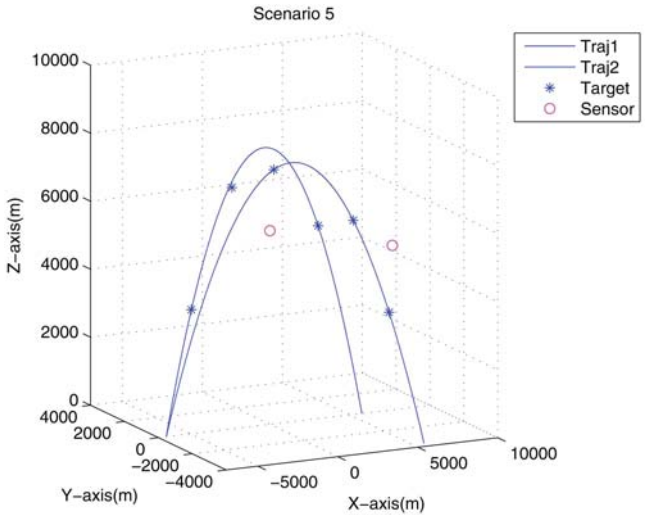

Fig. 15. Scenario 5 for the two-sensor case.

TABLE V
Sensor positions (in m) for the scenarios considered.

	First Sensor			Second Sensor		
Scenario	ξ	η	ζ	ξ	η	ζ
1	−4550	5420	−945	6170	4250	−2700
2	−4550	5420	950	6170	4250	−2700
3	−4550	5420	950	6170	3250	−2700
4	−4550	5420	950	5170	4250	−2700
5	−1550	6120	−1445	6170	5250	−1400

2) Statistical Efficiency of the Estimates. In order to test for the statistical efficiency of the estimate (of the 23 dimensional vector), the NEES is used, with the CRLB as the covariance matrix. The sample average NEES over 100 Monte Carlo runs is shown in Figure 16 for all scenarios. The NEES is calculated using the FIM evaluated at both the true bias values and target positions, as well as at the estimated biases and target positions. The results are practically identical regardless of which values are chosen for evaluation of the FIM. The 95% probability region for the 100 sample average NEES of the 23 dimensional parameter vector is $[21.68, 24.34]$. For all five scenarios these NEES are found to be within this interval and the MLE is therefore statistically efficient. Figure 17 shows the individual bias component NEES for all scenarios, The 95% probability region for the 100 sample average single component NEES is $[0.74, 1.29]$. For all five scenarios these NEES are found to be within this interval.

The RMS position errors for the six targets are summarized in Table VI. In this table, the first estimation scheme was established as a baseline using bias-free LOS measurements to estimate the target positions. For the second scheme, we used biased LOS measurements but we only estimated target positions. In the last scheme, we used biased LOS measurements and we simultaneously estimated the target positions and sensor biases. For the second scheme, the estimation algorithm

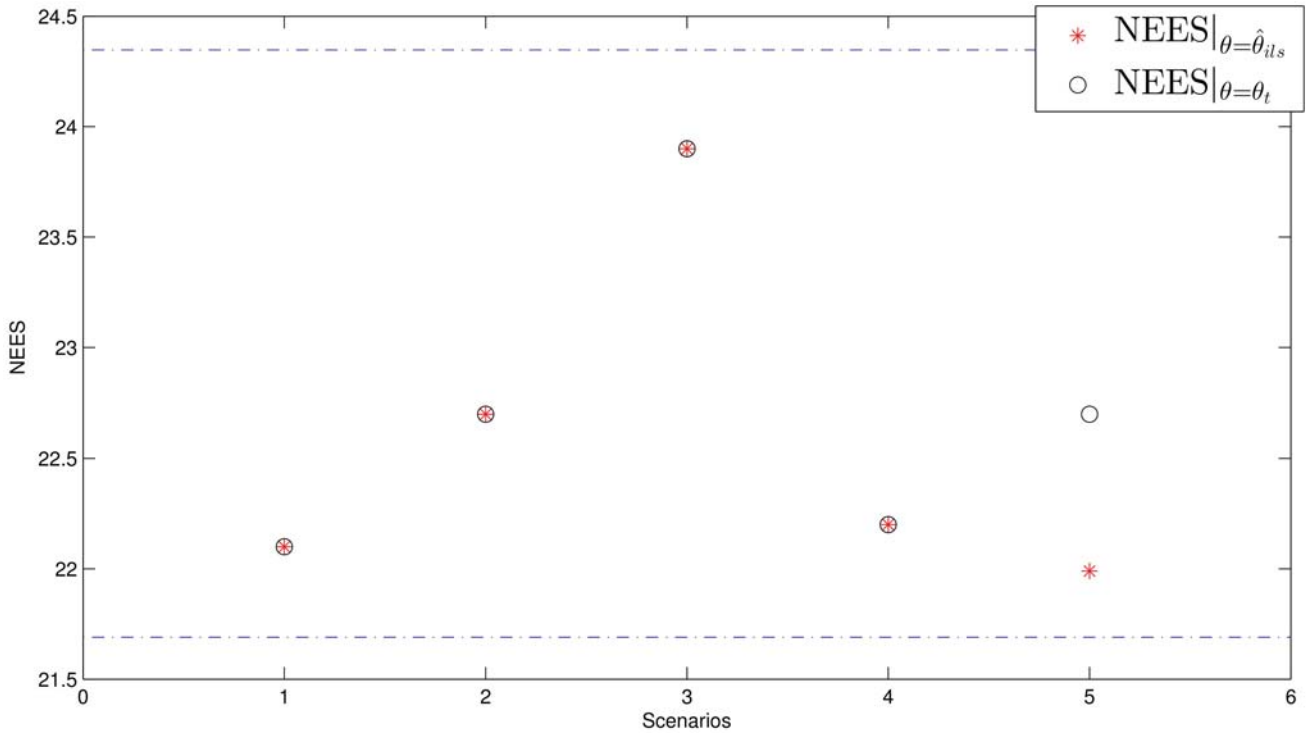

Fig. 16. Sample average NEES over 100 Monte Carlo runs for all five scenarios (two-sensor case).

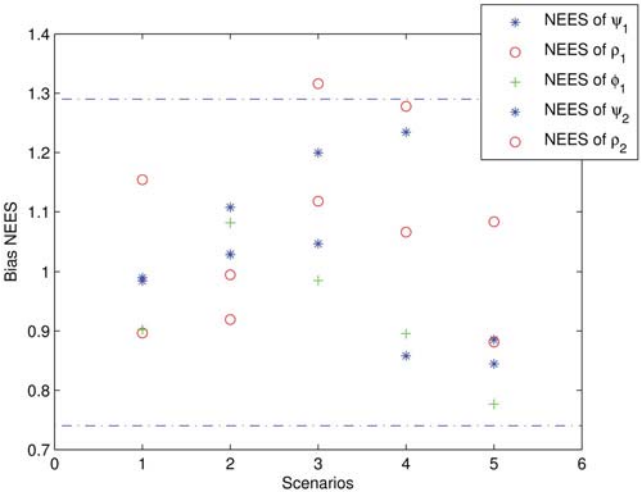

Fig. 17. Sample average bias NEES (CRLB evaluated at the estimate), for each of the five biases, over 100 Monte Carlo runs for all five scenarios (two-sensor case).

does not converge, while the third scheme shows satisfactory target RMS position errors in the presence of biases. The target position RMSE when the biases are also estimated, are close to the RMSE with no biases.

Each component of $\boldsymbol{\theta}$ should also be individually consistent with its corresponding σ_{CRLB} (the square root of the corresponding diagonal element of the inverse of FIM). In this case, the sample average bias RMSE over 100 Monte Carlo runs should be within 15% of its corresponding bias standard deviation from the CRLB (σ_{CRLB}) with 95% probability. Table VII demonstrates the efficiency of the individual bias estimates.

TABLE VI
Sample average position RMSE (in m) for the six targets, over 100 Monte Carlo runs, for the three estimation schemes (two-sensor case).

	First Target	Second Target	Third Target	Fourth Target	Fifth Target	Sixth Target
Scheme	RMSE	RMSE	RMSE	RMSE	RMSE	RMSE
1	3.68	4.84	3.42	4.06	4.64	3.63
3	7.08	7.65	6.49	7.91	7.70	7.76

TABLE VII
Sample average bias RMSE over 100 Monte Carlo runs and the corresponding bias standard deviation from the CRLB, for all configurations (in mrad) (two-sensor case).

		First Sensor			Second Sensor	
Scenario		ψ	ρ	ϕ	ψ	ρ
1	RMSE	0.195	0.271	0.254	0.186	0.314
	σ_{CRLB}	0.252	0.307	0.331	0.238	0.430
2	RMSE	0.437	0.442	0.500	0.428	0.348
	σ_{CRLB}	0.394	0.494	0.441	0.410	0.410
3	RMSE	1.675	1.668	1.634	1.646	0.4615
	σ_{CRLB}	1.279	1.572	1.305	1.207	0.536
4	RMSE	0.475	0.392	0.440	0.465	0.287
	σ_{CRLB}	0.467	0.440	0.510	0.483	0.384
5	RMSE	0.258	0.251	0.237	0.245	0.195
	σ_{CRLB}	0.345	0.246	0.357	0.347	0.168

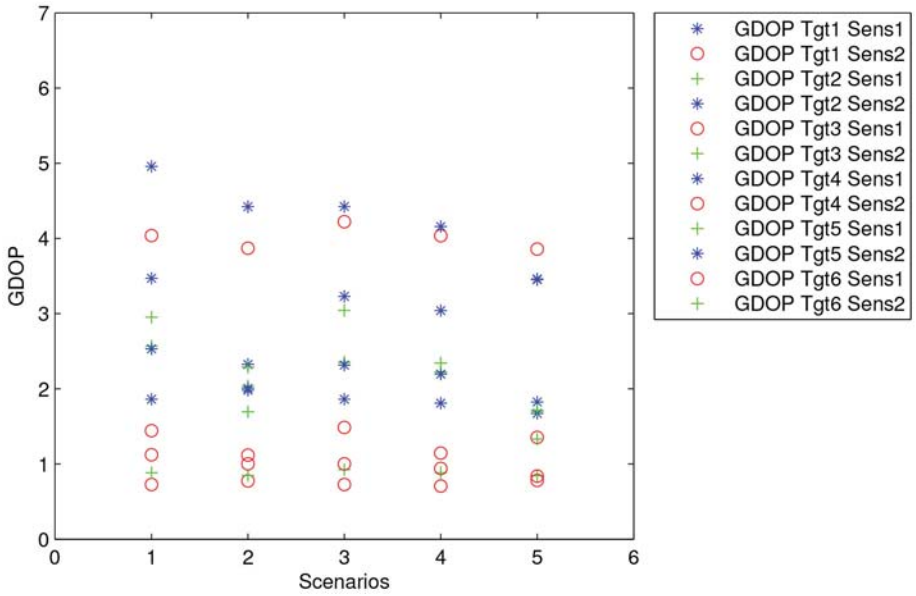

Fig. 18. GDOPs for the five scenarios considered (two-sensor case).

TABLE VIII
Sample average bias error $\bar{\tilde{b}}$ over $N = 100$ Monte Carlo runs for all configurations (in mrad) (to confirm that the bias estimates are unbiased) (two-sensor case).

Scenario		First Sensor			Second Sensor	
		ψ	ρ	ϕ	ψ	ρ
1	$\bar{\tilde{b}}$	0.000	0.007	0.000	0.003	−0.045
	$\frac{\sigma_{\text{CRLB}}}{\sqrt{N}}$	0.025	0.030	0.033	0.023	0.043
2	$\bar{\tilde{b}}$	−0.055	−0.058	−0.007	−0.016	−0.001
	$\frac{\sigma_{\text{CRLB}}}{\sqrt{N}}$	0.039	0.049	0.044	0.041	0.041
3	$\bar{\tilde{b}}$	−0.351	−0.098	−0.254	0.275	0.056
	$\frac{\sigma_{\text{CRLB}}}{\sqrt{N}}$	0.128	0.157	0.130	0.120	0.053
4	$\bar{\tilde{b}}$	−0.001	−0.069	0.042	−0.026	−0.013
	$\frac{\sigma_{\text{CRLB}}}{\sqrt{N}}$	0.046	0.044	0.051	0.048	0.038
5	$\bar{\tilde{b}}$	0.037	0.028	0.006	0.040	−0.005
	$\frac{\sigma_{\text{CRLB}}}{\sqrt{N}}$	0.034	0.024	0.0358	0.034	0.016

To confirm that the bias estimates are unbiased, the average bias error $\bar{\tilde{b}}$, from Table VIII, over 100 Monte Carlo runs confirms that $|\bar{\tilde{b}}|$ is less then $2\sigma_{\text{CRLB}}/\sqrt{N}$ (which it should be with 95% probability), i.e., these estimates are unbiased.

Figure 18 shows the various GDOP levels in the 12 target-sensor combinations for each of the five scenarios for which statistical efficiency was confirmed, in the case of the two sensors.

IV. CONCLUSIONS AND FUTURE WORK

In this paper, we presented an algorithm that uses targets of opportunity for estimation of measurement biases. The first step was formulating a general bias model for synchronized optical sensors at fixed known locations. The association of measurements is assumed to be perfect. Based on this, we used a ML approach that led to a nonlinear least-squares estimation problem for simultaneous estimation of the 3D Cartesian positions of the targets of opportunity and the angle measurement biases of the sensors. The bias estimates, obtained via ILS, were shown to be unbiased and statistically efficient. In the three-sensor case it was shown that one has complete observability of the sensor biases. In the two-sensor case a rank deficiency of 1 in the FIM was observed, i.e., this allows estimation of only 5 out of 6 biases. A suitable geometric explanation was provided for this. For moving sensors this problem is expected to go away if the sensors move sufficiently.

APPENDIX

The appropriate partial derivatives of (20) are

$$\frac{\partial g_{1_{is}}}{\partial x_k} = \frac{\partial g_{1_{is}}}{\partial x_{is}}\frac{\partial x_{is}}{\partial x_k} + \frac{\partial g_{1_{is}}}{\partial y_{is}}\frac{\partial y_{is}}{\partial x_k} + \frac{\partial g_{1_{is}}}{\partial z_{is}}\frac{\partial z_{is}}{\partial x_k} \tag{45}$$

$$\frac{\partial g_{1_{is}}}{\partial y_k} = \frac{\partial g_{1_{is}}}{\partial x_{is}}\frac{\partial x_{is}}{\partial y_k} + \frac{\partial g_{1_{is}}}{\partial y_{is}}\frac{\partial y_{is}}{\partial y_k} + \frac{\partial g_{1_{is}}}{\partial z_{is}}\frac{\partial z_{is}}{\partial y_k} \tag{46}$$

$$\frac{\partial g_{1_{is}}}{\partial z_k} = \frac{\partial g_{1_{is}}}{\partial x_{is}}\frac{\partial x_{is}}{\partial z_k} + \frac{\partial g_{1_{is}}}{\partial y_{is}}\frac{\partial y_{is}}{\partial z_k} + \frac{\partial g_{1_{is}}}{\partial z_{is}}\frac{\partial z_{is}}{\partial z_k} \tag{47}$$

$$\frac{\partial g_{1_{is}}}{\partial \psi_k} = \frac{\partial g_{1_{is}}}{\partial x_{is}}\frac{\partial x_{is}}{\partial \psi_k} + \frac{\partial g_{1_{is}}}{\partial y_{is}}\frac{\partial y_{is}}{\partial \psi_k} + \frac{\partial g_{1_{is}}}{\partial z_{is}}\frac{\partial z_{is}}{\partial \psi_k} \tag{48}$$

$$\frac{\partial g_{1_{is}}}{\partial \rho_k} = \frac{\partial g_{1_{is}}}{\partial x_{is}}\frac{\partial x_{is}}{\partial \rho_k} + \frac{\partial g_{1_{is}}}{\partial y_{is}}\frac{\partial y_{is}}{\partial \rho_k} + \frac{\partial g_{1_{is}}}{\partial z_{is}}\frac{\partial z_{is}}{\partial \rho_k} \tag{49}$$

$$\frac{\partial g_{1_{is}}}{\partial \phi_k} = \frac{\partial g_{1_{is}}}{\partial x_{is}}\frac{\partial x_{is}}{\partial \phi_k} + \frac{\partial g_{1_{is}}}{\partial y_{is}}\frac{\partial y_{is}}{\partial \phi_k} + \frac{\partial g_{1_{is}}}{\partial z_{is}}\frac{\partial z_{is}}{\partial \phi_k} \tag{50}$$

$$\frac{\partial g_{2_{is}}}{\partial x_k} = \frac{\partial g_{2_{is}}}{\partial x_{is}}\frac{\partial x_{is}}{\partial x_k} + \frac{\partial g_{2_{is}}}{\partial y_{is}}\frac{\partial y_{is}}{\partial x_k} + \frac{\partial g_{2_{is}}}{\partial z_{is}}\frac{\partial z_{is}}{\partial x_k} \tag{51}$$

$$\frac{\partial g_{2_{is}}}{\partial y_k} = \frac{\partial g_{2_{is}}}{\partial x_{is}}\frac{\partial x_{is}}{\partial y_k} + \frac{\partial g_{2_{is}}}{\partial y_{is}}\frac{\partial y_{is}}{\partial y_k} + \frac{\partial g_{2_{is}}}{\partial z_{is}}\frac{\partial z_{is}}{\partial y_k} \quad (52)$$

$$\frac{\partial g_{2_{is}}}{\partial z_k} = \frac{\partial g_{2_{is}}}{\partial x_{is}}\frac{\partial x_{is}}{\partial z_k} + \frac{\partial g_{2_{is}}}{\partial y_{is}}\frac{\partial y_{is}}{\partial z_k} + \frac{\partial g_{2_{is}}}{\partial z_{is}}\frac{\partial z_{is}}{\partial z_k} \quad (53)$$

$$\frac{\partial g_{2_{is}}}{\partial \psi_k} = \frac{\partial g_{2_{is}}}{\partial x_{is}}\frac{\partial x_{is}}{\partial \psi_k} + \frac{\partial g_{2_{is}}}{\partial y_{is}}\frac{\partial y_{is}}{\partial \psi_k} + \frac{\partial g_{2_{is}}}{\partial z_{is}}\frac{\partial z_{is}}{\partial \psi_k} \quad (54)$$

$$\frac{\partial g_{2_{is}}}{\partial \rho_k} = \frac{\partial g_{2_{is}}}{\partial x_{is}}\frac{\partial x_{is}}{\partial \rho_k} + \frac{\partial g_{2_{is}}}{\partial y_{is}}\frac{\partial y_{is}}{\partial \rho_k} + \frac{\partial g_{2_{is}}}{\partial z_{is}}\frac{\partial z_{is}}{\partial \rho_k} \quad (55)$$

$$\frac{\partial g_{2_{is}}}{\partial \phi_k} = \frac{\partial g_{2_{is}}}{\partial x_{is}}\frac{\partial x_{is}}{\partial \phi_k} + \frac{\partial g_{2_{is}}}{\partial y_{is}}\frac{\partial y_{is}}{\partial \phi_k} + \frac{\partial g_{2_{is}}}{\partial z_{is}}\frac{\partial z_{is}}{\partial \phi_k} \quad (56)$$

Given that (2) can be written as

$$\mathbf{x}_{is} = \begin{bmatrix} x_{is} \\ y_{is} \\ z_{is} \end{bmatrix} = T_s(\mathbf{x}_i - \boldsymbol{\xi}_s) = \begin{bmatrix} T_{s_{11}} & T_{s_{12}} & T_{s_{13}} \\ T_{s_{21}} & T_{s_{22}} & T_{s_{23}} \\ T_{s_{31}} & T_{s_{32}} & T_{s_{33}} \end{bmatrix} \begin{bmatrix} x_i - \xi_s \\ y_i - \eta_s \\ z_i - \zeta_s \end{bmatrix} \quad (57)$$

therefore

$$x_{is} = T_{s_{11}}(x_i - \xi_s) + T_{s_{12}}(y_i - \eta_s) + T_{s_{13}}(z_i - \zeta_s) \quad (58)$$

$$y_{is} = T_{s_{21}}(x_i - \xi_s) + T_{s_{22}}(y_i - \eta_s) + T_{s_{23}}(z_i - \zeta_s) \quad (59)$$

$$z_{is} = T_{s_{31}}(x_i - \xi_s) + T_{s_{32}}(y_i - \eta_s) + T_{s_{33}}(z_i - \zeta_s) \quad (60)$$

and

$$\begin{aligned} \frac{\partial x_{is}}{\partial x_k} &= T_{s_{11}}, \quad \frac{\partial x_{is}}{\partial y_k} = T_{s_{12}}, \quad \frac{\partial x_{is}}{\partial y_k} = T_{s_{13}} \\ \frac{\partial y_{is}}{\partial x_k} &= T_{s_{21}}, \quad \frac{\partial y_{is}}{\partial y_k} = T_{s_{22}}, \quad \frac{\partial y_{is}}{\partial y_k} = T_{s_{23}} \\ \frac{\partial z_{is}}{\partial x_k} &= T_{s_{31}}, \quad \frac{\partial z_{is}}{\partial y_k} = T_{s_{32}}, \quad \frac{\partial z_{is}}{\partial y_k} = T_{s_{33}} \end{aligned} \quad (61)$$

$$\frac{\partial x_{is}}{\partial \psi_k} = \frac{\partial T_{s_{11}}}{\partial \psi_k}(x_i - \xi_s) + \frac{\partial T_{s_{12}}}{\partial \psi_k}(y_i - \eta_s) + \frac{\partial T_{s_{13}}}{\partial \psi_k}(z_i - \zeta_s) \quad (62)$$

$$\frac{\partial x_{is}}{\partial \rho_k} = \frac{\partial T_{s_{11}}}{\partial \rho_k}(x_i - \xi_s) + \frac{\partial T_{s_{12}}}{\partial \rho_k}(y_i - \eta_s) + \frac{\partial T_{s_{13}}}{\partial \rho_k}(z_i - \zeta_s) \quad (63)$$

$$\frac{\partial x_{is}}{\partial \phi_k} = \frac{\partial T_{s_{11}}}{\partial \phi_k}(x_i - \xi_s) + \frac{\partial T_{s_{12}}}{\partial \phi_k}(y_i - \eta_s) + \frac{\partial T_{s_{13}}}{\partial \phi_k}(z_i - \zeta_s) \quad (64)$$

$$\frac{\partial y_{is}}{\partial \psi_k} = \frac{\partial T_{s_{21}}}{\partial \psi_k}(x_i - \xi_s) + \frac{\partial T_{s_{22}}}{\partial \psi_k}(y_i - \eta_s) + \frac{\partial T_{s_{23}}}{\partial \psi_k}(z_i - \zeta_s) \quad (65)$$

$$\frac{\partial y_{is}}{\partial \rho_k} = \frac{\partial T_{s_{21}}}{\partial \rho_k}(x_i - \xi_s) + \frac{\partial T_{s_{22}}}{\partial \rho_k}(y_i - \eta_s) + \frac{\partial T_{s_{23}}}{\partial \rho_k}(z_i - \zeta_s) \quad (66)$$

$$\frac{\partial y_{is}}{\partial \phi_k} = \frac{\partial T_{s_{11}}}{\partial \phi_k}(x_i - \xi_s) + \frac{\partial T_{s_{22}}}{\partial \phi_k}(y_i - \eta_s) + \frac{\partial T_{s_{23}}}{\partial \phi_k}(z_i - \zeta_s) \quad (67)$$

$$\frac{\partial z_{is}}{\partial \psi_k} = \frac{\partial T_{s_{31}}}{\partial \psi_k}(x_i - \xi_s) + \frac{\partial T_{s_{32}}}{\partial \psi_k}(y_i - \eta_s) + \frac{\partial T_{s_{33}}}{\partial \psi_k}(z_i - \zeta_s) \quad (68)$$

$$\frac{\partial z_{is}}{\partial \rho_k} = \frac{\partial T_{s_{31}}}{\partial \rho_k}(x_i - \xi_s) + \frac{\partial T_{s_{32}}}{\partial \rho_k}(y_i - \eta_s) + \frac{\partial T_{s_{33}}}{\partial \rho_k}(z_i - \zeta_s) \quad (69)$$

$$\frac{\partial z_{is}}{\partial \phi_k} = \frac{\partial T_{s_{31}}}{\partial \phi_k}(x_i - \xi_s) + \frac{\partial T_{s_{32}}}{\partial \phi_k}(y_i - \eta_s) + \frac{\partial T_{s_{33}}}{\partial \phi_k}(z_i - \zeta_s) \quad (70)$$

$$\frac{\partial g_{1_{is}}}{\partial x_{is}} = \frac{z_{is}}{z_{is}^2 + x_{is}^2} \quad (71)$$

$$\frac{\partial g_{1_{is}}}{\partial y_{is}} = 0 \quad (72)$$

$$\frac{\partial g_{1_{is}}}{\partial z_{is}} = -\frac{x_{is}}{x_{is}^2 + z_{is}^2} \quad (73)$$

$$\frac{\partial g_{2_{is}}}{\partial x_{is}} = -\frac{x_{is}y_{is}}{\sqrt{(x_{is}^2 + z_{is}^2)}(x_{is}^2 + y_{is}^2 + z_{is}^2)} \quad (74)$$

$$\frac{\partial g_{2_{is}}}{\partial y_{is}} = \frac{\sqrt{x_{is}^2 + z_{is}^2}}{x_{is}^2 + y_{is}^2 + z_{is}^2} \quad (75)$$

$$\frac{\partial g_{2_{is}}}{\partial z_{is}} = -\frac{z_{is}y_{is}}{(x_{is}^2 + y_{is}^2 + z_{is}^2)\left(\sqrt{x_{is}^2 + z_{is}^2}\right)} \quad (76)$$

$$\frac{\partial T_{s_{11}}}{\partial \psi_k} = -\sin\psi_k \cos\rho_k \quad (77)$$

$$\frac{\partial T_{s_{12}}}{\partial \psi_k} = -\sin\psi_k \sin\rho_k \sin\phi_k - \cos\psi_k \cos\phi_k \quad (78)$$

$$\frac{\partial T_{s_{13}}}{\partial \psi_k} = -\sin\psi_k \sin\rho_k \cos\phi_k + \cos\psi_k \sin\phi_k \quad (79)$$

$$\frac{\partial T_{s_{21}}}{\partial \psi_k} = \cos\psi_k \cos\rho_k \quad (80)$$

$$\frac{\partial T_{s_{22}}}{\partial \psi_k} = \cos\psi_k \sin\rho_k \sin\phi_k - \sin\psi_k \cos\phi_k \quad (81)$$

$$\frac{\partial T_{s_{23}}}{\partial \psi_k} = \cos\psi_k \sin\rho_k \cos\phi_k + \sin\psi_k \sin\phi_k \quad (82)$$

$$\frac{\partial T_{s_{31}}}{\partial \psi_k} = 0 \quad (83)$$

$$\frac{\partial T_{s_{32}}}{\partial \psi_k} = 0 \quad (84)$$

$$\frac{\partial T_{s_{33}}}{\partial \psi_k} = 0 \quad (85)$$

$$\frac{\partial T_{s_{11}}}{\partial \rho_k} = -\cos\psi_k \sin\rho_k \tag{86}$$

$$\frac{\partial T_{s_{12}}}{\partial \rho_k} = \cos\psi_k \cos\rho_k \sin\phi_k \tag{87}$$

$$\frac{\partial T_{s_{13}}}{\partial \rho_k} = \cos\psi_k \cos\rho_k \cos\phi_k \tag{88}$$

$$\frac{\partial T_{s_{21}}}{\partial \rho_k} = -\sin\psi_k \sin\phi_k \tag{89}$$

$$\frac{\partial T_{s_{22}}}{\partial \rho_k} = \sin\psi_k \cos\rho_k \sin\phi_k \tag{90}$$

$$\frac{\partial T_{s_{23}}}{\partial \rho_k} = \sin\psi_k \cos\rho_k \cos\phi_k \tag{91}$$

$$\frac{\partial T_{s_{31}}}{\partial \rho_k} = -\cos\phi_k \tag{92}$$

$$\frac{\partial T_{s_{32}}}{\partial \rho_k} = -\sin\rho_k \sin\phi_k \tag{93}$$

$$\frac{\partial T_{s_{33}}}{\partial \rho_k} = -\sin\rho_k \cos\phi_k \tag{94}$$

$$\frac{\partial T_{s_{11}}}{\partial \phi_k} = 0 \tag{95}$$

$$\frac{\partial T_{s_{12}}}{\partial \phi_k} = \cos\psi_k \sin\rho_k \cos\phi_k + \sin\psi_k \sin\phi_k \tag{96}$$

$$\frac{\partial T_{s_{13}}}{\partial \phi_k} = -\cos\psi_k \sin\rho_k \sin\phi_k + \sin\psi_k \cos\phi_k \tag{97}$$

$$\frac{\partial T_{s_{21}}}{\partial \phi_k} = 0 \tag{98}$$

$$\frac{\partial T_{s_{22}}}{\partial \phi_k} = \sin\psi_k \sin\rho_k \cos\phi_k - \cos\psi_k \sin\phi_k \tag{99}$$

$$\frac{\partial T_{s_{23}}}{\partial \phi_k} = -\sin\psi_k \sin\rho_k \sin\phi_k - \cos\psi_k \cos\phi_k \tag{100}$$

$$\frac{\partial T_{s_{31}}}{\partial \phi_k} = 0 \tag{101}$$

$$\frac{\partial T_{s_{32}}}{\partial \phi_k} = \cos\psi_k \cos\phi_k \tag{102}$$

$$\frac{\partial T_{s_{33}}}{\partial \phi_k} = -\cos\rho_k \sin\phi_k \tag{103}$$

REFERENCES

[1] Y. Bar-Shalom, X.-R. Li, and T. Kirubarajan
Estimation with Applications to Tracking and Navigation: Theory, Algorithms and Software.
J. Wiley and Sons, 2001.

[2] Y. Bar-Shalom, P. K. Willett, and X. Tian
Tracking and Data Fusion.
YBS Publishing, 2011.

[3] D. Belfadel, R. W. Osborne, and Y. Bar-Shalom
"A Minimalist Approach to Bias Estimation for Passive Sensor Measurements with Targets of Opportunity,"
in *Proc. SPIE Conf. Signal and Data Processing of Small Targets*, #8857-13, San Diego, California, Aug. 2013.

[4] D. Belfadel, R. W. Osborne, and Y. Bar-Shalom
"Bias Estimation for Optical Sensor Measurements with Targets of Opportunity,"
in *Proc. 16th International Conference on Information Fusion*, Istanbul, Turkey, Jul. 2013.

[5] X. Benlian and W. Zhiquan
"Biased Bearings-Only Parameter Estimation for Bistatic System,"
Journal of Electronics (China), vol. 24, no. 3, May 2007.

[6] S. V. Bordonaro, P. Willett, and Y. Bar-Shalom
"Tracking with Converted Position and Doppler Measurements,"
in *Proc. SPIE Conf. Signal and Data Processing of Small Targets*, #8137-12, San Diego, CA, Aug. 2011.

[7] S. V. Bordonaro, P. Willett, and Y. Bar-Shalom
"Consistent Linear Tracker with Position and Range Rate Measurements,"
in *Proc. Asilomar Conf.*, Asilomar, CA, Nov. 2012.

[8] S. V. Bordonaro, P. Willett, and Y. Bar-Shalom
"Unbiased Tracking with Converted Measurements,"
in *Proc. 2012 IEEE Radar Conf.*, Atlanta, GA, May 2012.

[9] S. V. Bordonaro, P. Willett, and Y. Bar-Shalom
"Unbiased Tracking with Converted Measurements,"
in *Proc. 51st IEEE Conf. on Decision and Control*, Maui, HI, Dec. 2012.

[10] D. F. Crouse, R. Osborne, III, K. Pattipati, P. Willett, and Y. Bar-Shalom
"2D Location Estimation of Angle-Only Sensor Arrays Using Targets of Opportunity,"
in *Proc. 13th International Conference on Information Fusion*, Edinburgh, Scotland, Jul. 2010.

[11] B. D. Kragel, S. Danford, S. M. Herman, and A. B. Poore
"Bias Estimation Using Targets of Opportunity,"
Proc. SPIE Conf. on Signal and Data Processing of Small Targets, #6699, Aug. 2007.

[12] B. D. Kragel, S. Danford, S. M. Herman, and A. B. Poore
"Joint MAP Bias Estimation and Data Association: Algorithms,"
Proc. SPIE Conf. on Signal and Data Processing of Small Targets, #6699-1E, Aug. 2007.

[13] B. D. Kragel, S. Danford, and A. B. Poore
"Concurrent MAP Data Association and Absolute Bias Estimation with an Arbitrary Number of Sensors,"
Proc. SPIE Conf. on Signal and Data Processing of Small Targets, #6969-50, May 2008.

[14] X. Lin, F. Y. Bar-Shalom, and T. Kirubarajan
"Exact Multisensor Dynamic Bias Estimation with Local Tracks,"
IEEE Trans. on Aerospace and Electronic Systems, vol. 40, no. 2, pp. 576–590, Apr. 2004.

[15] R. W. Osborne, III, and Y. Bar-Shalom
"Statistical Efficiency of Composite Position Measurements from Passive Sensors,"
in *Proc. SPIE Conf. on Signal Proc., Sensor Fusion, and Target Recognition*, #8050-07, Orlando, FL, Apr. 2011.

[16] R. W. Osborne, III, and Y. Bar-Shalom
"Statistical Efficiency of Composite Position Measurements from Passive Sensors,"
IEEE Trans. on Aerospace and Electronic Systems, vol. 49, no. 4, Oct. 2013.

Djedjiga Belfadel is a Ph.D. candidate in the Electrical Engineering department at the University of Connecticut, Storrs, CT. Her research interests include target tracking, data association, sensor fusion, sensor biases, machine vision, and other aspects of estimation. She obtained her B.S., degrees from the University of Mouloud Mammeri in 2003, and her M.S., degrees from the University of New Haven in 2008, both in electrical engineering. Before joining the Estimation and Signal Processing (ESP) Laboratory, she worked, as an Electrical Engineer, from 2009 to 2011, at Evax Systems Inc. in Branford, Connecticut.

Richard W. Osborne, III obtained his B.S., M.S., and Ph.D. degrees in electrical engineering from the University of Connecticut in 2004, 2007, and 2012, respectively. He is currently an Assistant Research Professor in the Electrical Engineering department at the University of Connecticut, Storrs, CT. His academic interests include adaptive target tracking, information/sensor fusion, machine vision, and other aspects of estimation.

Yaakov Bar-Shalom was born on May 11, 1941. He received the B.S. and M.S. degrees from the Technion, Israel Institute of Technology, in 1963 and 1967 and the Ph.D. degree from Princeton University in 1970, all in electrical engineering. From 1970 to 1976 he was with Systems Control, Inc., Palo Alto, California. Currently he is Board of Trustees Distinguished Professor in the Dept. of Electrical and Computer Engineering and Marianne E. Klewin Professor in Engineering at the University of Connecticut. He is also Director of the ESP (Estimation and Signal Processing) Lab. His current research interests are in estimation theory, target tracking and data fusion. He has published over 500 papers and book chapters in these areas and in stochastic adaptive control. He coauthored the monograph Tracking and Data Association (Academic Press, 1988), the graduate texts Estimation and Tracking: Principles, Techniques and Software (Artech House, 1993), Estimation with Applications to Tracking and Navigation: Algorithms and Software for Information Extraction (Wiley, 2001), the advanced graduate texts Multitarget-Multisensor Tracking: Principles and Techniques (YBS Publishing, 1995), Tracking and Data Fusion (YBS Publishing, 2011), and edited the books Multitarget-Multisensor Tracking: Applications and Advances (Artech House, Vol. I, 1990; Vol. II, 1992; Vol. III, 2000). He has been elected Fellow of IEEE for "contributions to the theory of stochastic systems and of multi-target tracking." He has been consulting to numerous companies and government agencies, and originated the series of Multitarget-Multisensor Tracking short courses offered via UCLA Extension, at Government Laboratories, private companies and overseas. During 1976 and 1977 he served as Associate Editor of the IEEE Transactions on Automatic Control and from 1978 to 1981 as Associate Editor of Automatica. He was Program Chairman of the 1982 American Control Conference, General Chairman of the 1985 ACC, and Co-Chairman of the 1989 IEEE International Conference on Control and Applications. During 1983–87 he served as Chairman of the Conference Activities Board of the IEEE Control Systems Society and during 1987–89 was a member of the Board of Governors of the IEEE CSS. He was a member of the Board of Directors of the International Society of Information Fusion (1999–2004) and served as General Chairman of FUSION 2000, President of ISIF in 2000 and 2002 and Vice President for Publications in 2004–13. In 1987 he received the IEEE CSS Distinguished Member Award. Since 1995 he is a Distinguished Lecturer of the IEEE AESS and has given numerous keynote addresses at major national and international conferences. He is co-recipient of the M. Barry Carlton Award for the best paper in the IEEE Transactions on Aerospace and Electronic Systems in 1995 and 2000 and recipient of the 1998 University of Connecticut AAUP Excellence Award for Research. In 2002 he received the J. Mignona Data Fusion Award from the DoD JDL Data Fusion Group. He is a member of the Connecticut Academy of Science and Engineering. In 2008 he was awarded the IEEE Dennis J. Picard Medal for Radar Technologies and Applications, and in 2012 the Connecticut Medal of Technology. He has been listed by academic.research.microsoft (top authors in engineering) as #1 among the researchers in Aerospace Engineering based on the citations of his work.